


Structure of twin boundaries of cholesteric blue phase I

Akihiro Yamashita (山下晃弘) and Jun-ichi Fukuda (福田順一) 

Department of Physics, Kyushu University, 744 Motoooka, Nishi-ku, Fukuoka 819-0395, Japan



(Received 7 October 2021; accepted 6 April 2022; published 25 April 2022)

We investigate numerically the structure of twin boundaries of cholesteric blue phases. Our study is based on the Landau–de Gennes continuum theory describing the orientational order of the liquid crystal by a second-rank tensor. We pay particular attention to blue phase I (BP I) with body-centered-cubic symmetry and consider twin boundaries between BP I lattices in which their (110) planes are shared and the $(\bar{1}12)$ plane of one lattice is parallel to the $(1\bar{1}2)$ plane of the other as observed in previous experiments [Jin *et al.*, *Sci. Adv.* **6**, eaay5986 (2020); Zhang *et al.*, *ACS Appl. Mater. Interf.* **13**, 36130 (2021)]. We discuss two plausible cases in which the twin boundaries are parallel to the {112} planes or the {111} planes. In the former, disclination lines of obtusely bent form penetrate the twin boundaries, and in the latter straight disclination lines as well as bent ones are found at the twin boundaries. The former twin boundaries are energetically less costly, consistent with previous experimental identifications. From our numerical results the free energy of a twin boundary per unit area is estimated to be $\simeq 4 \times 10^{-6} \text{ J m}^{-2}$, which indeed indicates that the formation of twin boundaries is not prohibitively costly.

DOI: [10.1103/PhysRevE.105.044707](https://doi.org/10.1103/PhysRevE.105.044707)

I. INTRODUCTION

Crystal lattices cannot be perfect unless prepared with great care, and imperfections of a crystal lattice, such as vacancies, dislocations of crystal lattice ordering, and disclinations of lattice orientation, influence significantly the macroscopic, in particular mechanical properties of the crystal [1,2]. Crystal twinning is another typical example of crystal imperfections, in which two separate crystal lattices of different lattice orientations coexist and share a crystal lattice plane [3–5]. Twinning of crystalline lattices occur in diffusionless martensitic transformations [6,7] and therefore has drawn interest from the viewpoint of engineering as well as from academic point of view.

Twinning of atomic crystals has been extensively studied for a long time, and recently soft materials with specific crystallographic symmetry (mainly cubic symmetry) have been attracting interest as a system exhibiting twinning of the underlying crystallographic ordering [8,9]. In twin boundaries of atomic crystals, the crystal lattices constituting the twin boundary share the atoms there, which puts a stringent constraint on the relative position and orientation of the constituent crystal lattices, known as the twin law. On the other hand, in soft materials with crystalline order, no discrete units like atoms occupy the “crystal lattice,” but self-organized positional and/or orientational order of constituent molecules exhibits crystalline symmetry; constituent molecules occupy the space in a continuous manner in the mesoscopic scale. Therefore there can be a richer possibility of the structures of twin boundaries in soft materials. Indeed, in the investigation of twin boundaries in bicontinuous cubic structures of

surfactants, Han *et al.* [8] considered their possible structures by varying the position of one cubic lattice with respect to the other in their theoretical model.

Here we focus on the structures of twin boundaries of cubic cholesteric blue phases. Cholesteric blue phases [10–13] are complex three-dimensional ordered structures exhibited by chiral liquid crystals and comprise an array of topological line defects of orientational order (disclination lines) and interwoven double twist cylinders in which the orientational order is twisted along all the directions perpendicular to the cylinder axis [Fig. 1(a)]. Two cubic blue phases are known; blue phase I (BP I) possesses body-centered-cubic symmetry and BP II simple-cubic symmetry (A third BP III is believed to be amorphous). The arrangement of disclination lines and double-twist cylinders is shown in Figs. 1(b) and 1(c) for BP I and BP II, respectively.

Very recently it was shown by microscope observations and numerical calculations that the structural transition from carefully prepared monocrystalline BP II to BP I is martensitic in the sense that the reorganization of the double-twist cylinder array is collective and diffusionless [14]. The resulting texture of BP I is indeed highly similar to that of martensites of atomic crystals with twin boundaries. A subsequent study based on x-ray scattering [9] revealed the relative orientation of twinned BP I lattices in which their (110) planes are shared and the $(\bar{1}12)$ plane of one lattice is parallel to the $(1\bar{1}2)$ plane of the other. A more recent study using Kossel diagrams confirmed the same twinning behavior and also observed the response of twinned BP I crystal to an applied electric field [15]. These studies indicate that crystalline order of soft materials provide an intriguing platform for the investigation of martensitic transformations and associated twin boundaries.

However, scattering experiments do not give information on the real-space structures of twin boundaries. Moreover, in

*fukuda.jun-ichi@phys.kyushu-u.ac.jp

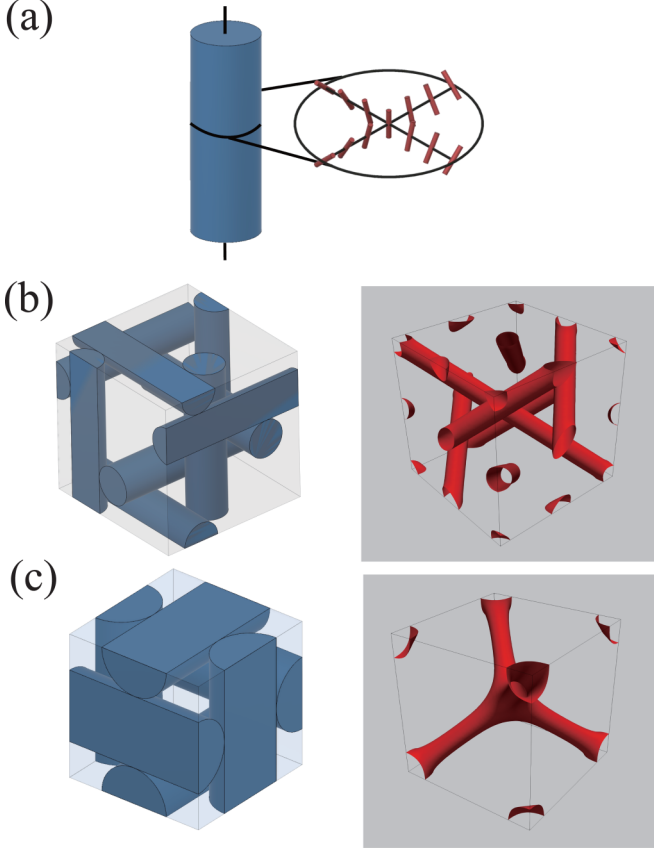


FIG. 1. (a) Schematic illustration of a double-twist cylinder. Short rods represent the orientation profile in a plane perpendicular to the cylinder axis. [(b) and (c)] Arrangement of double-twist cylinders (left) and disclination lines (right) in (b) BP I and (c) BP II.

addition to the absence of discrete units as in atomic crystals already mentioned above, the absence of mirror symmetry could complicate the investigation of twin boundaries of cholesteric blue phases; previous knowledge on twin boundaries of atomic crystals often relies on the presence of mirror symmetry. Here, motivated by the experimental finding of twinning of BP I [9,14,15], we investigate possible structures of twin boundaries of BP I numerically using the Landau–de Gennes continuum theory describing the orientational order by a second-rank tensor. The Landau–de Gennes theory has been successfully applied to cholesteric blue phases since the pioneering analytic studies of Hornreich and Shtrikman [12,16,17] and extensively employed in numerical studies (pioneering ones include those by Dupuis *et al.* [18] and by Alexander and Yeomans [19]). In Sec. II, we describe the Landau–de Gennes theory and the setup of our numerical calculations. In Sec. III we present and discuss the results of our calculations. We conclude this paper in Sec. IV.

II. MODEL

A. Free energy

In the framework of the Landau–de Gennes theory, we minimize the free energy as a functional of the tensor order parameter χ_{ij} to determine the structures of cholesteric blue

phases containing twin boundaries. We show here the essential part of our numerical calculations and refer to our previous work [20–23] for technical details.

The free energy of the liquid crystal is written as $F = \int dx dy dz [\varphi_{\text{local}}(\chi) + \varphi_{\text{elastic}}(\chi, \nabla)]$, where

$$\varphi_{\text{local}}(\chi) = \tau \text{Tr} \chi^2 - \sqrt{6} \text{Tr} \chi^3 + (\text{Tr} \chi^2)^2 \quad (1)$$

is the local free-energy density with Tr being the trace of a tensor, and

$$\varphi_{\text{elastic}}(\chi, \nabla) = \kappa^2 \{ [(\nabla \times \chi)_{ij} + \chi_{ij}]^2 + \eta [(\nabla \cdot \chi)_i]^2 \} \quad (2)$$

is the elastic energy involving spatial derivatives. Here summations over repeated indices are implied, $(\nabla \times \chi)_{ij} \equiv \epsilon_{ikl} \partial_k \chi_{lj}$ and $(\nabla \cdot \chi)_i \equiv \partial_j \chi_{ij}$. Free-energy densities, length and the orientational order parameter itself have been rescaled [12,23] so that only three dimensionless parameters appear in Eqs. (1) and (2): τ is the rescaled temperature, κ is the strength of chirality, and η concerns the anisotropy of elasticity. We choose $\tau = -1.0$, $\kappa = 0.7$, and $\eta = 1$ (corresponding to one-constant approximation), for which BP I is thermodynamically stable [20]. The length is rescaled so that the cholesteric pitch p is 4π . The p before rescaling is $\simeq 160$ nm for $\kappa = 0.7$ [23]. In the following calculations periodic boundary conditions are employed, and hence no surface anchoring energy is involved in the total free energy.

We denote the rescaled free energy per unit area by $\mathcal{F} \equiv F / \int dx dy$. Then the free energy per unit area before rescaling, denoted by $\overline{\mathcal{F}}$, reads [23] $\overline{\mathcal{F}} \simeq \mathcal{F} \times 1.4 \times 10^{-18} \text{ J}/(\kappa^3 p^2)$. Using the above-mentioned $\kappa = 0.7$ and $p \simeq 160$ nm, we have

$$\overline{\mathcal{F}} \simeq \mathcal{F} \times 1.6 \times 10^{-4} \text{ J m}^{-2}. \quad (3)$$

We will use Eq. (3) for the evaluation of the free energy of twin boundaries given later, although the numerical value appearing in Eq. (3) depends on the material parameters in the free-energy density before rescaling (see Ref. [23] for the parameters used here).

B. Calculation of the orientation profile of bulk BP I

The orientation profile of bulk BP I and its lattice constant a have to be obtained for the following calculations of twin boundaries. For this purpose, the equilibrium profile of a unit cell of BP I and the resulting free-energy density $f = F/\overline{a}^3$ are calculated for fixed \overline{a} , and the optimum lattice constant a is determined by \overline{a} that minimizes f . The equilibrium profile is obtained by relaxing the orientation profile from the initial profile for the high-chirality limit (see Sec. VI.G of Ref. [12], or Eq. (9) of Ref. [18]). The numerical lattice is a cubic one with its axes (the x , y , and z axes) parallel to the cubic symmetry axes of BP I. Periodic boundary conditions are imposed. We use the following simple relaxation equation:

$$\frac{\partial}{\partial t} \chi_{ij}(\mathbf{r}) = -\frac{\delta F}{\delta \chi_{ij}(\mathbf{r})} - \lambda(\mathbf{r}) \delta_{ij}, \quad (4)$$

where $\lambda(\mathbf{r})$ is the Lagrange multiplier that ensures $\text{Tr} \chi = 0$ and t is the dimensionless time appropriately rescaled by the rotational viscosity (as we are now interested in equilibrium profiles rather than dynamics, the actual value of the rotational viscosity is not important). The explicit Euler scheme with the

time interval $\Delta t = 0.02$ is employed for the discretization of Eq. (4) with respect to t , and the discretization of the spatial derivatives follows the procedures in Ref. [20]. The obtained optimum lattice constant a is 4π , or the natural pitch, within 1% precision, and in the following calculations a is set to 4π .

C. Calculation of the orientation profiles containing twin boundaries

In the previous experiments demonstrating the twinning of BP I [9,14,15], the liquid crystal was sandwiched by patterned or photoaligned surfaces that imposed specific lattice orientation. However, we employ periodic boundary conditions in all the x , y , and z directions to avoid possible complications arising from the presence of confining surfaces and the associated surface anchoring. Note that periodic boundaries enforce the presence of two twin boundaries between two lattices with different orientations, as depicted in Fig. 2.

In all the calculations we will present below, the lattice orientations of BP I are chosen such that their (110) plane is parallel to the xy plane, and one of the $\{112\}$ planes is parallel to the yz plane. This setup is consistent with the experimentally found lattice orientations of BP I involving twin boundaries [9]. The thickness (or to be precise, the distance between two periodic boundaries) in the z direction is set to $\sqrt{2}a$, so that the numerical system accommodates one unit BP I lattice in the z direction.

In the case of atomic crystals, when the relative orientation of two crystal lattices is such that they share one of the $\{112\}$ planes of each lattice, the twin boundaries are parallel to either one of the $\{112\}$ planes or one of the $\{111\}$ planes. Although the absence of discrete units in our case of blue phases allows different possibility of the orientation of the twin boundaries, in the present study we restrict ourselves to the above-mentioned two cases in which twin boundaries are parallel to one of the $\{112\}$ planes or one of the $\{111\}$ planes (referred to as “ $\{112\}$ case” and “ $\{111\}$ case,” respectively, in the following). The numerical systems for these two cases are depicted in Figs. 2(a) and 2(b), respectively. The systems sizes, $2\sqrt{6}a \times \sqrt{3}a \times \sqrt{2}a$ in the $\{112\}$ case and $\sqrt{6}a \times 2\sqrt{3}a \times \sqrt{2}a$ in the $\{111\}$ case, have been chosen so that the periodicities imposed by the periodic boundaries conform to those of the inclined BP I lattices. The system dimension perpendicular to the twin boundaries is large enough for the two twin boundaries to be regarded safely as distinct but small enough for the calculations to be carried out with reasonable amount of numerical resources.

As mentioned in the Introduction, the BP I lattice does not possess “lattice points” as discrete units like atoms, and therefore the position of a twin boundary with respect to the BP I is not restricted as in the cases of atomic crystals. Nevertheless, for the convenience of the following discussions, we define the “lattice points” of the BP I lattice by the vertices and the body center of the unit cell shown in Fig. 2(c). We start our calculations with initial profiles in which the lattice points are shared by the two BP I lattices with different orientations (blue and green regions in Fig. 2), referred to as a “reference initial profile” in the following, and let the system relax by Eq. (4) to find an equilibrium profile. We seek the possibilities of twin boundaries with different structures by shifting one of the

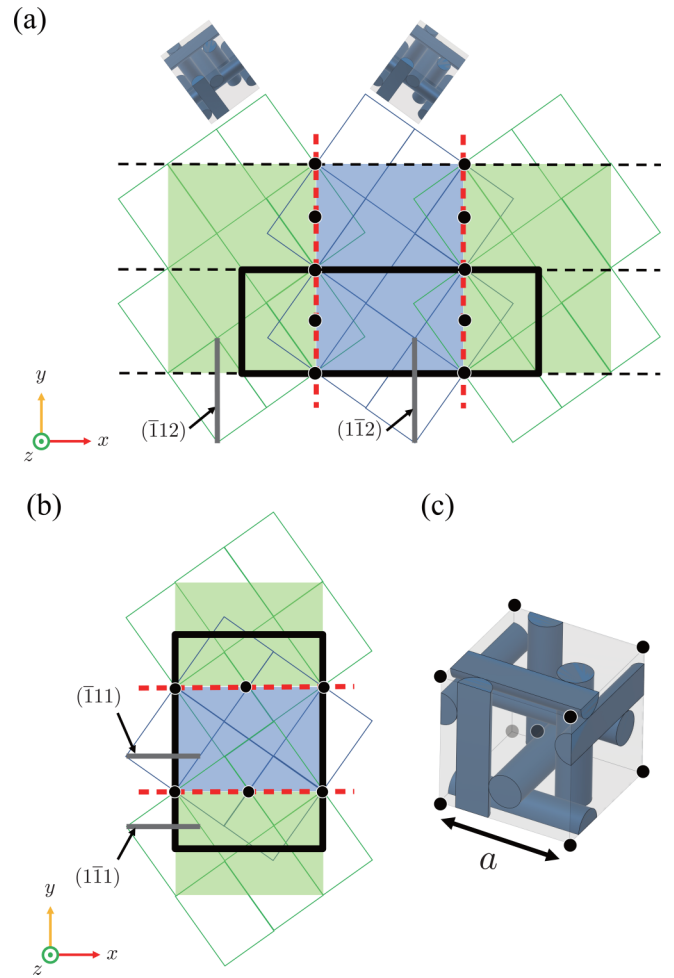


FIG. 2. [(a) and (b)] Numerical systems for (a) the $\{112\}$ case and (b) the $\{111\}$ case. In both cases, the (110) lattice plane is parallel to the plane of the figure. The region in which numerical calculations are carried out is depicted by a rectangle with thick black edges, whose size in the xy plane is (a) $2\sqrt{6}a \times \sqrt{3}a$ and (b) $\sqrt{6}a \times 2\sqrt{3}a$. Thick black edges represent periodic boundaries. Green and blue regions (lighter-shaded and darker-shaded regions in the print version) are filled with BP I lattices with their (110) plane parallel to the plain of the figure. Different lattice orientation in each region is specified by the schematic illustrations with double-twist cylinders on the top of panel (a). Apparently separated green (lighter-shaded in print) regions are in fact identical because of the periodic boundaries. Twin boundaries, depicted by thick red dashed lines, are parallel to (a) the yz plane and (b) the xz plane. Black dots depict the “lattice points” shared by lattices of different orientation. Black dashed horizontal lines in (a) emphasize the periodicity in the y direction. (c) “Lattice points” of body-centered-cubic BP I (black dots) and the lattice constant a .

lattices in the reference initial profile, and let the system relax. The lattice to be shifted is a green one in Figs. 2(a) and 2(b). Figure 3 illustrates how the green lattice is shifted. The initial condition for Eq. (4) is $\chi_{ij} = 0$ at the twin boundaries [red dashed lines Figs. 2(a) and 2(b)], and the values of χ obtained for bulk BP I in Sec. II B otherwise [appropriate rotations and translations of the bulk profile obtained in Sec. II B are applied to realize the lattice arrangement in Figs. 2(a) and 2(b)]. Note

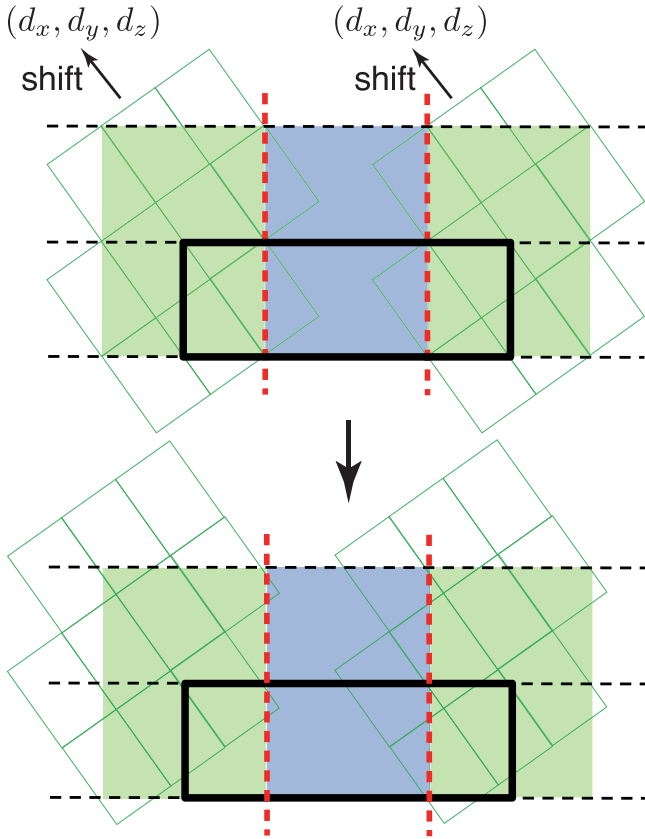


FIG. 3. Illustration of how the lattice in the green region is shifted from the “reference initial profile” (top) by (d_x, d_y, d_z) . The lattice in the blue region is now shown for clarity. Note again that the lattices in the green regions are identical under periodic boundary. Refer to the caption of Fig. 2 for colors.

that while the axes of cubic symmetry of BP I in Sec. II B are parallel to the x , y , and z axes of the numerical system, they are not in Fig. 2(a) and 2(b)].

III. RESULTS AND DISCUSSIONS

Here we show the calculation results particularly focusing on the arrangement of disclination lines and double-twist cylinders. We visualize disclination lines by drawing isosurfaces with $\text{Tr}\chi^2 = 1$ (note that $\text{Tr}\chi^2 \simeq 1.5$ far away from the disclination, and the orientational order is weakened at the cores of the disclinations [24]). See the Appendix for the visualization of the axes of double-twist cylinders.

A. $\{112\}$ cases

In Fig. 4, we show the profile of BP I with twin boundaries relaxed from the reference initial profile described in Sec. II C for the $\{112\}$ case. Here and in the following, orthographic projection is employed for the clarity of the presentation, and the Supplemental Material [25] provides figures of the same structures in perspective view. It is clearly seen that some of the disclination lines do not traverse the twin boundaries and are acutely bent there and that double-twist cylinders are disrupted at one of the twin boundaries. This profile looks unfavorable because in Bulk BP I, all the disclination lines

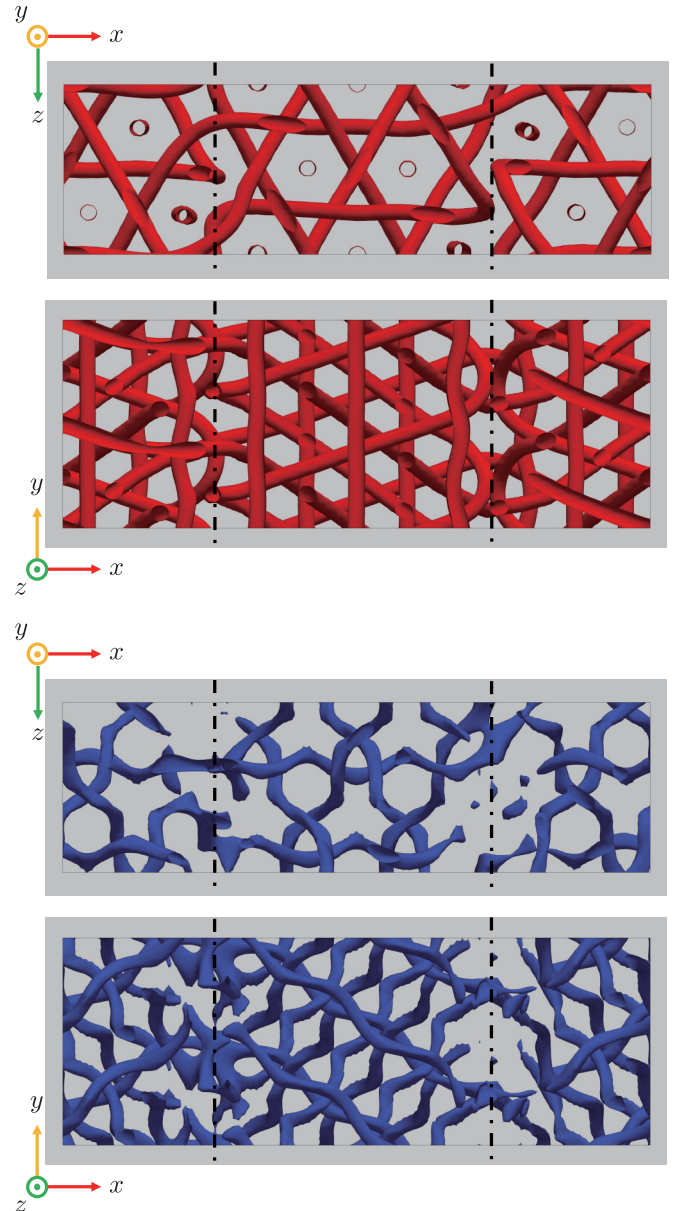


FIG. 4. The profile of BP I containing twin boundaries relaxed from the reference initial condition for the $\{112\}$ case. Top two and bottom two panels show disclination lines and axes of double-twist cylinders, respectively, viewed from different directions specified by the coordinate axes. The location of the twin boundaries is highlighted by dot-dashed lines. Here and in the following, the profiles are shown with orthographic projection, and in Supplemental Material [25], they are presented in perspective view.

are straight, and double-twist cylinders also span the whole system without interruption.

As mentioned in Sec. II C, we seek the profiles of twin boundaries with lower free energy by preparing an initial condition with the green lattice of Fig. 2(a) shifted by (d_x, d_y, d_z) from the reference initial profile (Fig. 3). From the symmetry argument, the ranges of d_x , d_y , and d_z can be limited to $0 \leq d_x < \sqrt{6}a/3$, $0 \leq d_y < \sqrt{3}a/2$, and $0 \leq d_z < \sqrt{2}a/2$. We eventually find that the profile relaxed from $(d_x, d_y, d_z) = (\sqrt{6}a/4, 0, \sqrt{2}a/4)$ gives the lowest free energy. The obtained

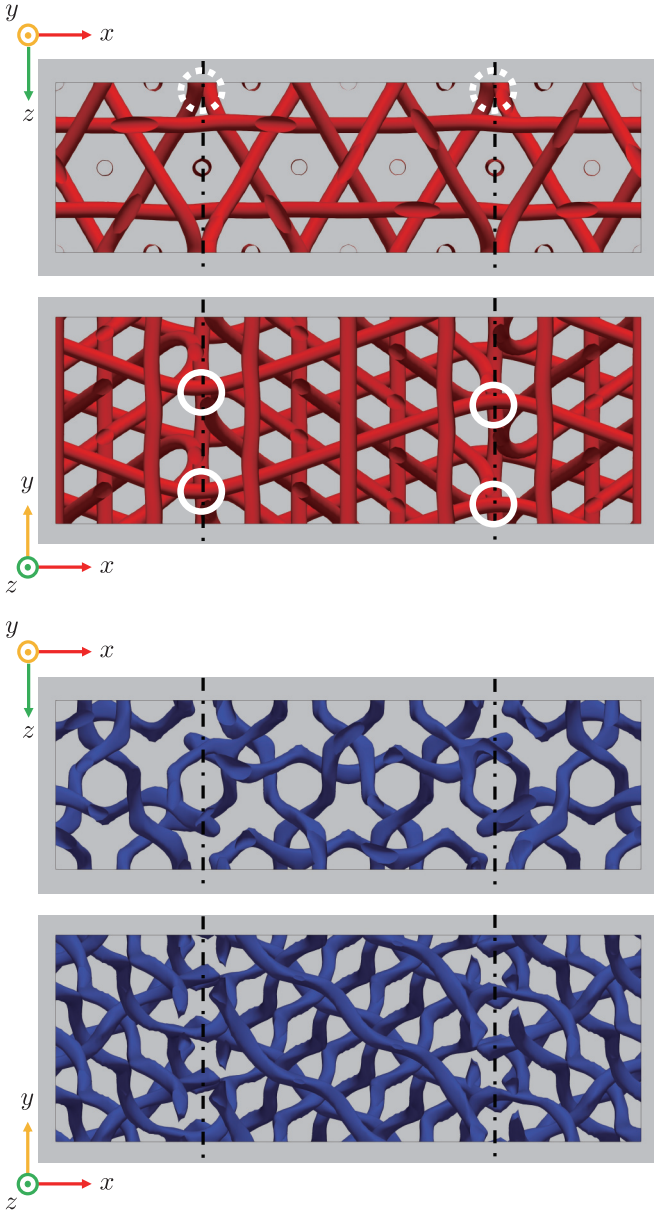


FIG. 5. The same as Fig. 4, except that the left part of the initial condition (connected to the right part by a periodic boundary) is shifted by $(d_x, d_y, d_z) = (\sqrt{6}a/4, 0, \sqrt{2}a/4)$ from the reference initial condition. Solid and dotted circles highlight the bending of disclination lines whose bending angle is $\cos^{-1}(-7/9) \simeq 141^\circ$ and $\cos^{-1}(-1/3) \simeq 109^\circ$, respectively (disclination lines at dotted circles continue through the periodic boundaries).

profile is shown in Fig. 5. In contrast to those in Fig. 4, disclination lines at the twin boundaries in Fig. 5 are obtusely bent. The bending angles can be evaluated from the orientation of disclination lines in the initial profile that would constitute the bent disclination line in the relaxed profile. The bending angles marked by solid circles and dotted circles in Fig. 5 are $\cos^{-1}(-7/9) \simeq 141^\circ$ and $\cos^{-1}(-1/3) \simeq 109^\circ$, respectively. The latter angle is exhibited by disclination lines that go back to the original lattice without traversing the twin boundaries. Despite the small angle compared to that exhibited by traversing disclination lines, the distortion of the disclination

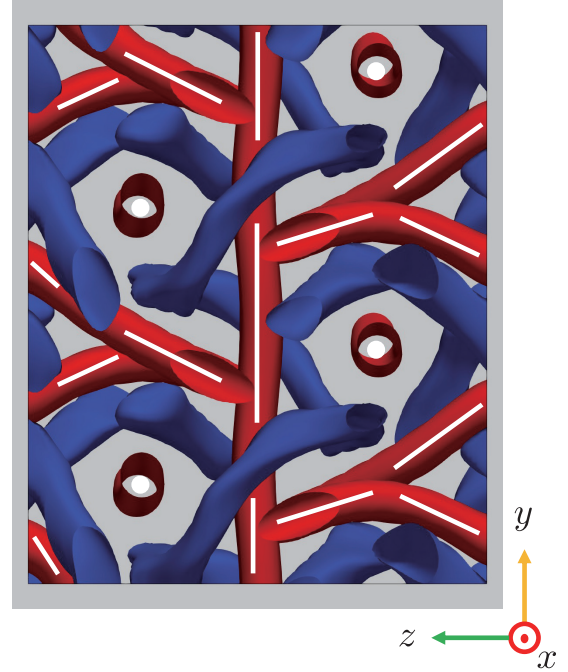


FIG. 6. Detailed structure of a twin boundary in Fig. 5 over the thickness $(\sqrt{6}/5) \times 4\pi \simeq 0.49a$. Disclination lines (red, marked by white lines) and axes of double-twist cylinders (blue) are shown simultaneously. The structure of one twin boundary there is the same as that of the other.

network at the twin boundaries is quite small, as can be seen in Fig. 5.

The two twin boundaries in Fig. 5 are identical, and the bent parts of the disclination lines traversing the twin boundaries lie in the xz plane as the straight parts do; the disclination lines viewed from the y direction are almost indistinguishable from those in the bulk BP I without twin boundaries. Double-twist cylinders traverse the twin boundaries rather smoothly, in contrast to disrupted double-twist cylinders in Fig. 4. In Fig. 6, the detailed structure of one twin boundary in Fig. 5 is shown, which again confirms smooth traversing of double-twist cylinders and disclination lines.

The rescaled free energy of the whole numerical system [with volume being $2\sqrt{6}a \times \sqrt{3}a \times \sqrt{2}a = 12(4\pi)^3$] is calculated to be $F = -2.294049 \times 10^4$. The free energy of twin boundaries is estimated by subtracting F by the free energy of bulk BP I without twin boundaries. The latter for the same volume, from a separate calculation, is $F_{\text{bulk}} = -2.295966 \times 10^4$. Since the area of the twin boundaries in the system is $2 \times \sqrt{3}a \times \sqrt{2}a = 2\sqrt{6}(4\pi)^2$ (recall that two separate twin boundaries are present), from Eq. (3) the free energy of twin boundaries per unit area (before rescaling) is estimated to be

$$\begin{aligned} \bar{\mathcal{F}}_{\{112\}} &\simeq 1.6 \times 10^{-4} \\ &\times \frac{[-2.294049 - (-2.295966)] \times 10^4}{2\sqrt{6}(4\pi)^2} \text{ J m}^{-2} \\ &\simeq 4.0 \times 10^{-6} \text{ J m}^{-2}. \end{aligned} \quad (5)$$

To give a feeling about the magnitude of the free-energy density in Eq. (5), let us comment that $4.0 \times 10^{-6} \text{ J m}^{-2}$ is close to typical values for weak surface anchoring energy density. Therefore the formation of twin boundaries is not prohibitively costly, and thus indeed observed experimentally [9,15]. Although the resulting free-energy density (5) contains the interaction energy between two parallel twin boundaries, the “self-energy” is expected to be much larger, and therefore we believe that Eq. (5) gives a reasonable estimate of the free energy of twin boundaries.

B. {111} cases

Figure 7 shows the profile of BP I with twin boundaries relaxed from the reference initial profile described in Sec. II C for the {111} case. Complex arrangement of disclination lines and double-twist cylinders is seen at the twin boundaries, and some disclination lines are bent acutely there. As in Sec. III A, now we prepare an initial condition with the blue lattice of Fig. 2(b) shifted by (d_x, d_y, d_z) from the reference initial profile, and let it relax by Eq. (4). The range of d_x , d_y and d_z is the same as that presented in Sec. III A. We find that a profile with $(d_x, d_y, d_z) = (\sqrt{6}a/4, 3\sqrt{3}a/32, \sqrt{2}a/4)$ gives the minimum of the free energy, which is shown in Fig. 8. It is clearly seen that, in contrast to Fig. 7, straight disclination lines run along the y direction, which is naturally expected to be favorable energetically. Disclination lines that traverse the twin boundaries obliquely are bent there, with the bending angle of $\cos^{-1}(-5/9) \simeq 124^\circ$. Similarly to the previous case (Fig. 5), the disclination lines viewed from the y direction are close to those in the bulk BP I without twin boundaries. Arrangement of double-twist cylinders is much more naturally ordered than that in Fig. 7.

The two twin boundaries in Fig. 8 are identical, and their detailed structure is presented in Fig. 9. Interestingly, three-fold local rotational symmetry about the disclination lines normal to the twin boundary is found, although not perfect due to numerical artifacts (Recall the threefold rotational symmetry about the straight disclination lines of bulk BP I with cubic symmetry).

The rescaled free energy of the whole numerical system (with volume being $\sqrt{6}a \times 2\sqrt{3}a \times \sqrt{2}a = 12(4\pi)^3$, the same as that for the {112} case) is now calculated to be $F = -2.292155 \times 10^4$. Recalling that the area of the two twin boundaries is now $2 \times \sqrt{6}a \times \sqrt{2}a = 4\sqrt{3}(4\pi)^2$, as we did in Sec. III A, we can estimate the free energy of twin boundaries per unit area (before rescaling) for the present {111} case to be

$$\bar{\mathcal{F}}_{\{111\}} \simeq 5.6 \times 10^{-6} \text{ J m}^{-2}, \quad (6)$$

larger than $\bar{\mathcal{F}}_{\{112\}}$ presented in Sec. III A. This result indicates that twin boundaries parallel to the {112} planes are more preferable, consistent with the previous experimental identifications [9,15]. In the {112} case, the bend is smaller for disclination lines traversing the twin boundaries ($\simeq 141^\circ$, compared with $\simeq 124^\circ$ for the {111} case). Moreover, apparently small distortion of the disclination network is induced by disclination lines with small bend angle ($\simeq 109^\circ$) that do not traverse the twin boundaries. These observations could give an intuitive explanation on why twin boundaries parallel to

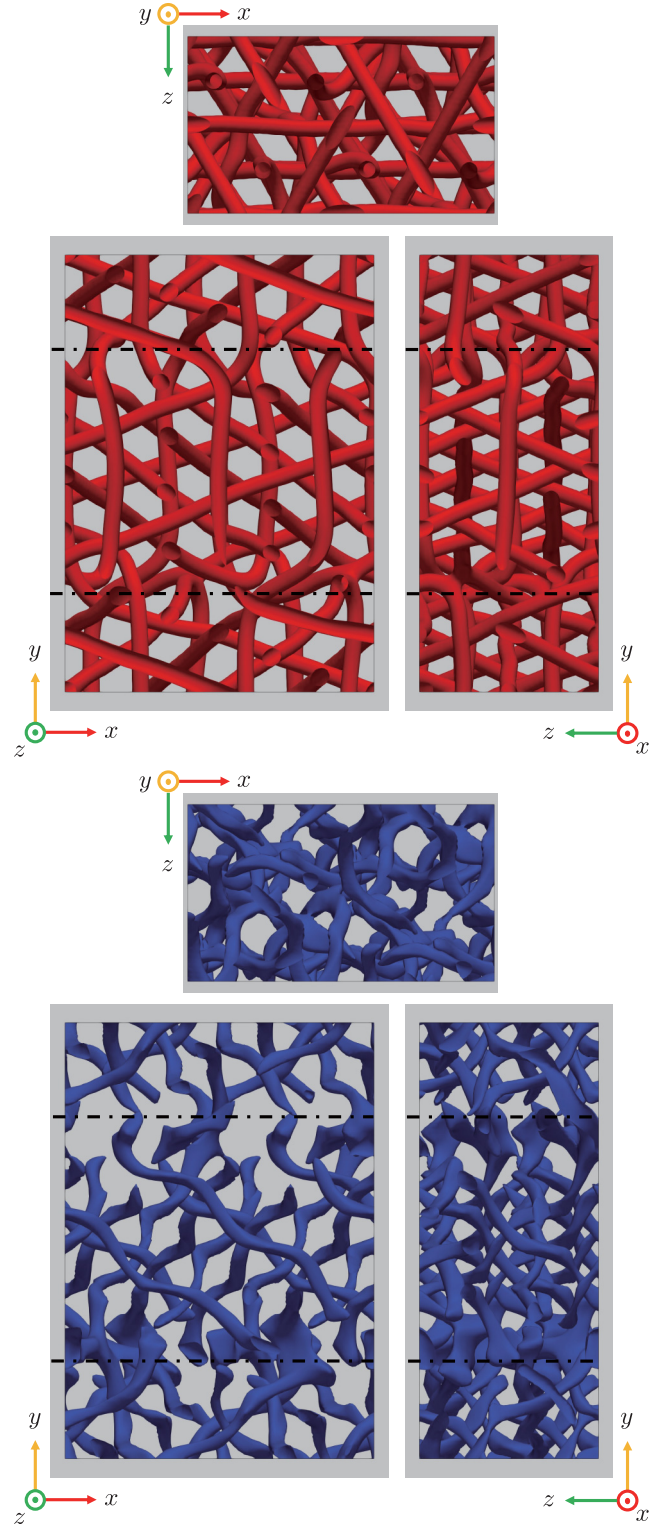


FIG. 7. The profile of BP I containing twin boundaries relaxed from the reference initial condition for the {111} case. Top two and bottom two panels show disclination lines and axes of double-twist cylinders, respectively, viewed from different directions specified by the coordinate axes.

the {112} planes are energetically more favorable than those parallel to the {111} planes.

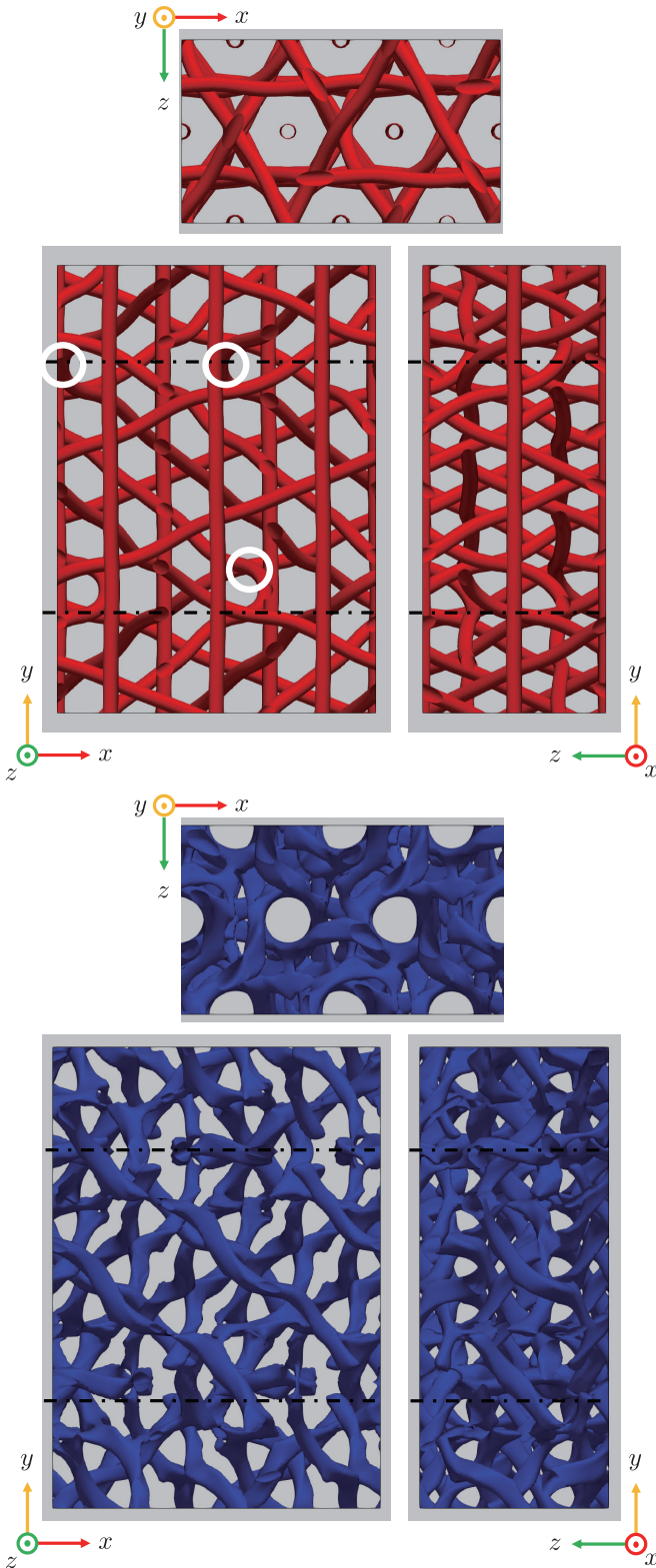


FIG. 8. The same as Fig. 7, except that the upper part of the initial condition (connected to the lower part by a periodic boundary) is shifted by $(d_x, d_y, d_z) = (\sqrt{6}a/4, 3\sqrt{3}a/32, \sqrt{2}a/4)$ from the reference initial condition. Here the profiles seen from the y direction are also shown to emphasize straight disclination lines along the y direction. Circles highlight the bending of disclination lines with the angle of $\cos^{-1}(-5/9) \simeq 124^\circ$ at the twin boundaries.

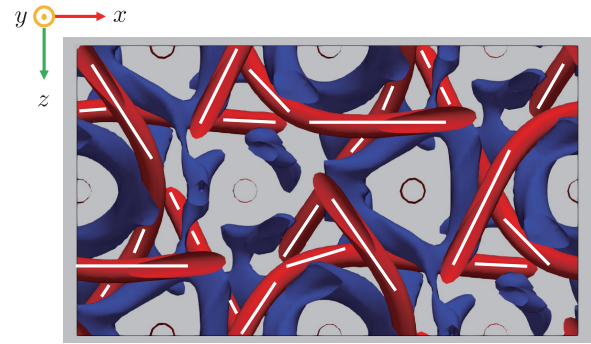


FIG. 9. Detailed structures of a twin boundary in Fig. 8, each over the thickness $(3\sqrt{3}/4) \times 4\pi \simeq 0.65a$. Disclination lines (red, marked by white lines) and axes of double-twist cylinders (blue) are shown simultaneously. The structure of one twin boundary there is the same as that of the other.

IV. CONCLUSIONS

Motivated by recent experiments that discovered martensitic transformation of cholesteric blue phase of a chiral liquid crystal, we investigated numerically the structure of twin boundaries of BP I. Our study is based on the Landau–de Gennes continuum theory with the orientational order parameter being a second-rank tensor χ_{ij} , and the free energy being given as a functional of χ_{ij} . We considered two plausible cases in which the twin boundaries is parallel to the $\{112\}$ planes and to the $\{111\}$ planes. In both cases we found the profiles of twin boundaries at which the disclination lines are connected there so that they are straight or obtusely bent. We also found that the free energy of a twin boundary is smaller when it is parallel to the $\{112\}$ planes, consistent with previous experimental identifications. The free energy per unit area is $\simeq 4 \times 10^{-6} \text{ J m}^{-2}$, which is small enough to allow the formation of twin boundaries in actual systems. We note that of course there can be twin boundaries other than those of the two cases mentioned above. However, the consideration of general cases requires a huge amount of numerical calculations with independent three-dimensional rotations of BP I lattices on both sides of the twin boundary (green and blue lattices in Fig. 2) in addition of translational shift. Strictly speaking, the above estimate of the free energy hence gives an upper limit of the minimum free energy. We still believe that it gives a reasonable estimate because twin boundaries with other plane orientations have not been observed experimentally.

Direct experimental observation of detailed structures of disclination lines of cholesteric blue phases is highly challenging, but real-space periodic structures of blue phases have indeed been experimentally observed by electron microscopy [26–28] and confocal microscopy [29]. In particular, non-destructive confocal microscopy with the aid of numerical generation of microscope images [30] might help the experimental elucidation of how the blue phase cubic lattices are connected at twin boundaries. We hope that our work will motivate further experimental studies to clarify the real-space ordering of twin boundaries of cholesteric blue phases, and also theoretical studies on the twin boundaries and imperfections (including dislocations [31] and disclinations) of cubic or other crystalline order of soft materials.

ACKNOWLEDGMENTS

The authors thank H. Yoshida and Y. Zhang for valuable discussions and suggestions that motivated this work. J.F. is grateful also to Yasushi Okumura for stimulating comments. This work is supported by JSPS KAKENHI (Grants No. JP17H02947 and No. JP21H01049).

APPENDIX: VISUALIZATION OF THE AXES OF DOUBLE-TWIST CYLINDERS

Our visualization of the axes of double-twist cylinders follows the procedure in Ref. [31]. In the following, the director \mathbf{n} at \mathbf{r} is taken to be the normalized eigenvector of $\chi_{ij}(\mathbf{r})$ with the largest eigenvalue.

We consider an ideal double-twist cylinder whose axis passes a certain point \mathbf{r} . Then $\mathbf{n}(\mathbf{r})$ is parallel to the cylinder axis, and we denote $\mathbf{n}(\mathbf{r})$ by \mathbf{n} in the following. The distance between a certain point \mathbf{r}' and the cylinder axis is

$$d(\mathbf{r}') = |(\mathbf{r}' - \mathbf{r}) - [(\mathbf{r}' - \mathbf{r}) \cdot \mathbf{n}]\mathbf{n}|. \quad (\text{A1})$$

Let $N(\mathbf{r}')$ denote the director of this ideal double-twist cylinder at \mathbf{r}' . The angle between \mathbf{n} (cylinder axis) and $N(\mathbf{r}')$ is

$$\theta(\mathbf{r}') = \frac{\pi}{2} \frac{d(\mathbf{r}')}{D}, \quad (\text{A2})$$

where D is the diameter of the double-twist cylinder. Thus $N(\mathbf{r}')$ is written as

$$N(\mathbf{r}') = \mathbf{n} \cos \theta(\mathbf{r}') + \mathbf{e}_\perp \sin \theta(\mathbf{r}'), \quad (\text{A3})$$

where $\mathbf{e}_\perp \equiv (\mathbf{r}' - \mathbf{r}) \times \mathbf{n} / |(\mathbf{r}' - \mathbf{r}) \times \mathbf{n}|$ is a unit vector perpendicular to the cylinder axis and in the plane spanned by $(\mathbf{r}' - \mathbf{r})$ and \mathbf{n} .

To determine whether a grid point \mathbf{r} on our numerical system is on or sufficiently close to one double-twist cylinder axis, we first calculate $N(\mathbf{r}')$ at the neighboring grid points \mathbf{r}' using Eq. (A3) and \mathbf{n} at \mathbf{r} . Let $N'(\mathbf{r}')$ denote the director determined from the numerically calculated profile $\chi_{ij}(\mathbf{r}')$. If \mathbf{r} is exactly on the axis of an ideal double-twist cylinder, $\cos^{-1}(|N(\mathbf{r}') \cdot N'(\mathbf{r}')|) = 0$ at every \mathbf{r}' . Thus, we define

$$A(\mathbf{r}) \equiv \sum_{\mathbf{r}' \in \text{NN}} \cos^{-1}(|N(\mathbf{r}') \cdot N'(\mathbf{r}')|), \quad (\text{A4})$$

where $\sum_{\mathbf{r}' \in \text{NN}}$ means that the summation is taken over the six nearest neighbors of \mathbf{r} . When $A(\mathbf{r})$ is sufficiently small, we judge that \mathbf{r} is sufficiently close to one double-twist cylinder axis. In our visualizations of double-twist cylinders in Figs. 4, and 5, 7, and 8, we show the isosurfaces $A(\mathbf{r}) = 0.2$. We note that after some trials and errors we have chosen $D = 0.35a$, where a is the lattice constant of BP I, although D should be $a/4$ if BP I is regarded as a regular pile of straight double-twist cylinders as shown in Fig. 1. Note also that, contrary to the straight shape commonly seen in schematic figures of cholesteric blue phases such as Fig. 1, double-twist cylinders look wavy not only in our systems containing twin boundaries but also in a bulk BP I, as visualized in Refs. [31,32].

-
- [1] L. Landau, E. Lifshitz, A. Kosevich, and L. Pitaevskii, *Theory of Elasticity*, Course of Theoretical Physics (Butterworth-Heinemann, Oxford, 1986).
- [2] T. H. Courtney, *Mechanical Behavior of Materials* (Waveland Press, Long Grove, IL, 2005).
- [3] M. V. Klassen-Neklyudova, *Mechanical Twinning of Crystals* (Consultant Bureau, New York, 1964).
- [4] T. Hahn and H. Klapper, Twinning of crystals, *International Tables for Crystallography* (Springer, Berlin, 2013), Chap. 3.3, pp. 413–483.
- [5] S. Parsons, Introduction to twinning, *Acta Crystallogr. D* **59**, 1995 (2003).
- [6] J. W. Christian, Twinning and martensitic transformation, *J. Phys. Colloq.* **35**, C7-65 (1974).
- [7] K. Bhattacharya *et al.*, *Microstructure of Martensite: Why It Forms and How It Gives Rise to the Shape-memory Effect*, Vol. 2 (Oxford University Press, Oxford, 2003).
- [8] L. Han, N. Fujita, H. Chen, C. Jin, O. Terasaki, and S. Che, Crystal twinning of bicontinuous cubic structures, *Int. Union Crystallogr. J.* **7**, 228 (2020).
- [9] H. M. Jin, X. Li, J. A. Dolan, R. J. Kline, J. A. Martínez-González, J. Ren, C. Zhou, J. J. de Pablo, and P. F. Nealey, Soft crystal martensites: An in situ resonant soft x-ray scattering study of a liquid crystal martensitic transformation, *Sci. Adv.* **6**, eaay5986 (2020).
- [10] H. Stegemeyer, T. Blümel, K. Hiltrop, H. Onusseit, and F. Porsch, Thermodynamic, structural and morphological studies on liquid-crystalline blue phases, *Liq. Cryst.* **1**, 3 (1986).
- [11] E. Dubois-violette and B. Pansu, Frustration and related topology of blue phases, *Mol. Cryst. Liq. Cryst.* **165**, 151 (1988).
- [12] D. C. Wright and N. D. Mermin, Crystalline liquids: The blue phases, *Rev. Mod. Phys.* **61**, 385 (1989).
- [13] C. Bahr and H.-S. Kitzerow, *Chirality in Liquid Crystals* (Springer, Berlin, 2001).
- [14] X. Li, J. A. Martínez-González, J. P. Hernández-Ortiz, A. Ramírez-Hernández, Y. Zhou, M. Sadati, R. Zhang, P. F. Nealey, and J. J. de Pablo, Mesoscale martensitic transformation in single crystals of topological defects, *Proc. Natl. Acad. Sci. USA* **114**, 10011 (2017).
- [15] Y. Zhang, H. Yoshida, S. Cho, J.-i. Fukuda, and M. Ozaki, In situ optical characterization of twinning in liquid crystalline blue phases, *ACS Appl. Mater. Interf.* **13**, 36130 (2021).
- [16] H. Grebel, R. M. Hornreich, and S. Shtrikman, Landau theory of cholesteric blue phases, *Phys. Rev. A* **28**, 1114 (1983).
- [17] R. M. Hornreich and S. Shtrikman, Landau theory of blue phases, *Mol. Cryst. Liq. Cryst.* **165**, 183 (1988).
- [18] A. Dupuis, D. Marenduzzo, and J. M. Yeomans, Numerical calculations of the phase diagram of cubic blue phases in cholesteric liquid crystals, *Phys. Rev. E* **71**, 011703 (2005).
- [19] G. P. Alexander and J. M. Yeomans, Stabilizing the blue phases, *Phys. Rev. E* **74**, 061706 (2006).
- [20] J.-i. Fukuda, M. Yoneya, and H. Yokoyama, Simulation of cholesteric blue phases using a Landau–de Gennes theory:

- Effect of an applied electric field, *Phys. Rev. E* **80**, 031706 (2009).
- [21] J. Fukuda and S. Žumer, Cholesteric blue phases: Effect of strong confinement, *Liq. Cryst.* **37**, 875 (2010).
- [22] A. Nych, J. Fukuda, U. Ognysta, S. Žumer, and I. Muševič, Spontaneous formation and dynamics of half-skyrmions in a chiral liquid-crystal film, *Nat. Phys.* **13**, 1215 (2017).
- [23] J.-i. Fukuda and S. Žumer, Lattice orientation of cholesteric blue phases in contact with surfaces enforcing unidirectional planar anchoring, *Phys. Rev. Research* **2**, 033407 (2020).
- [24] N. Schopohl and T. J. Sluckin, Defect Core Structure in Nematic Liquid Crystals, *Phys. Rev. Lett.* **59**, 2582 (1987).
- [25] See Supplemental Material at <http://link.aps.org/supplemental/10.1103/PhysRevE.105.044707> for the profiles in perspective view.
- [26] M. J. Costello, S. Meiboom, and M. Sammon, Electron microscopy of a cholesteric liquid crystal and its blue phase, *Phys. Rev. A* **29**, 2957 (1984).
- [27] S. Tanaka, H. Yoshida, Y. Kawata, R. Kuwahara, R. Nishi, and M. Ozaki, Double-twist cylinders in liquid crystalline cholesteric blue phases observed by transmission electron microscopy, *Sci. Rep.* **5**, 16180 (2015).
- [28] J. Liu, W. Liu, B. Guan, B. Wang, L. Shi, F. Jin, Z. Zheng, J. Wang, T. Ikeda, and L. Jiang, Diffusionless transformation of soft cubic superstructure from amorphous to simple cubic and body-centered cubic phases, *Nat. Commun.* **12**, 3477 (2021).
- [29] K. Higashiguchi, K. Yasui, and H. Kikuchi, Direct observation of polymer-stabilized blue phase I structure with confocal laser scanning microscope, *J. Am. Chem. Soc.* **130**, 6326 (2008).
- [30] J. Fukuda, Y. Okumura, and H. Kikuchi, Calculation of confocal microscope images of cholesteric blue phases, *Proc. SPIE* **9769**, 976906 (2016).
- [31] S. Wang, Structures of constrained blue phases: modelling and simulation, Ph.D. thesis, University of Ljubljana, 2019.
- [32] G. P. Alexander and J. M. Yeomans, Numerical results for the blue phases, *Liq. Cryst.* **36**, 1215 (2009).